RSC Advances

PAPER

View Article Online
View Journal | View Issue

Cite this: *RSC Adv.*, 2025, **15**, 8430

A calcium sulfate hemihydrate self-setting interface reinforced polycaprolactone porous composite scaffold

Changfeng Li,†[a] Dongying Li,†[ab] Yong Xu,[ab] Peng Chen,[a] Jianfei Zhang,[a] Yanrong Zhou,[a] Zonghan Li,[a] Zixiong Zhou,[a] Meigui Chen*[b] and Mengqi Li*[c]

The mechanical insufficiency and slow degradation of polycaprolactone (PCL) implants have attracted widespread attention among researchers. Herein, a PCL scaffold with self-setting properties containing calcium sulfate hemihydrate (CSH) was prepared using a triply periodic minimal surfaces (TPMS) design and selective laser sintering (SLS) technology. The results showed that the strength of the scaffold containing 10 wt% CSH was increased by 45.5% compared to the PCL one. More importantly, its strength can be further increased to 1.7 times that of the PCL scaffold after self-setting in water. Mechanism analysis suggests that mechanical strengthening can be attributed to the pinning effect through the newly grown columnar crystals embedded with PCL molecular chains. In addition, the degradation rate of the composite scaffold was approximately 6.8 times higher than that of the PCL one. The study believes that the increase in degradation rate is due to a dual effect, specifically the increase in permeability and the catalytic degradation of PCL in the acidic environment. Encouragingly, the composite scaffold showed a good ability to induce hydroxyapatite formation. Therefore, the self-setting mechanically enhanced composite scaffold is expected to have potential application prospects in bone defect repair.

Received 2nd January 2025
Accepted 9th March 2025

DOI: 10.1039/d5ra00010f

rsc.li/rsc-advances

1. Introduction

Artificial bone scaffolds have become an effective way to solve the problem of limited donors for traditional implants due to their wide range of material sources and adjustable biological and mechanical properties.[1–3] Polycaprolactone (PCL) as a bone scaffold material has good processability and biocompatibility, but pure PCL scaffolds have problems such as insufficient mechanical properties and slow degradation.[4,5]

Researchers have made various attempts to address the above issues. In order to promote bone regeneration and improve mechanical properties, Bagherzadeh *et al.* used the excellent mechanical strength and piezoelectric properties of polyvinylidene fluoride (PVDF) to prepare PCL/PVDF piezoelectric scaffolds by electrospinning. The mechanical properties and osteogenic ability of the composite scaffold were significantly improved, but the degradation rate was lower than that of the pure PCL scaffold.[6] Based on the advantages of gelatin (GL) such as good hydrophilicity and fast degradation, Gil-Castell *et al.* prepared PCL/GL scaffolds by electrospinning, which showed good degradability.[7] However, when Azarudeen *et al.* used 3D bioprinting to evaluate its mechanics, they discovered that the composite scaffold's tensile strength was lower than that of the PCL scaffold and decreased as the amount of GL increased.[8] These studies suggest that doping with other components with complementary advantages is an effective approach to address scaffold defects, but improving both degradation and mechanical properties simultaneously remains challenging.

Bioceramics have attracted widespread attention due to their sufficient bioactivity, biocompatibility and osteoconductivity.[9,10] Research shows that combining PCL with some bioceramics can improve the mechanical strength of PCL and have certain bioactivity.[11–13] Among the different types of bioceramics suitable for combining with PCL, calcium sulfate hemihydrate (CSH) is a good choice. It has good bioabsorbability and degradation properties, and can be converted into anhydrite (calcium sulfate dihydrate) to form a more stable hydrated form.[14,15] Zhou *et al.* prepared PCL/CSH composite fibers by electrospinning, which showed good tensile strength and bioactivity. They also unexpectedly found that the mechanics of the composite fibers were enhanced after water soaking, but without further research.[16] La Gatta *et al.* mixed modified PCL

[a]*College of Mechanical and Energy Engineering, Shaoyang University, Shaoyang, 422000, China*

[b]*Key Laboratory of Hunan Province for Efficient Power System and Intelligent Manufacturing, Shaoyang University, Shaoyang 422000, China. E-mail: chenmeigui@syxy247.wecom.work*

[c]*Shaoyang Industry Polytechnic College, Shaoyang 422000, China. E-mail: sciencefield@126.com*

† These authors contributed to the work equally and should be regarded as co-first authors.

with CSH and developed an injectable bone regeneration system. The PCL/CSH composites showed no cytotoxicity and better hydrophilicity than pure PCL material.[17] However, there is no research on the degradation of the composite scaffold, the micromorphology of the scaffold after self-curing mechanical enhancement, and the mechanical enhancement mechanism; secondly, as far as we know, there are few studies on the three-dimensional porous composite bone scaffold of this composite material.

In this work, selective laser sintering (SLS) technology was used to prepare PCL/CSH porous composite scaffolds with self-setting properties. The physical phase and tensile fracture morphology of CSH in the scaffold before and after soaking in a water medium were analyzed, and the self-setting enhancement mechanical mechanism was explored. The effect of CSH on scaffold degradation was discussed through the degradation surface morphology, weight loss, and solution pH value. In addition, the *in vitro* bioactivity of the composite scaffolds was evaluated.

2. Materials and methods

2.1 Structural design of scaffold model

The TPMS unit cell structures commonly used in regenerative medicine include I-WP, Schwarz P, Gyroid, Fischer-Koch S, Diamond, Double Diamond, *etc.* Since the I-WP unit cell structure has strong designability and excellent mechanical strength and can provide sufficient support, this paper chooses to use the I-WP unit cell type to construct the scaffold specimen.[18] To balance the mechanical strength, the porosity of the scaffold was set to 60%.[19,20] The tensile specimen standard was implemented according to GB/T 16421-1996 "Test Method for Small Specimens of Plastic Tensile Properties".[21] The dimensions of the tensile specimen were: 45 mm long, 3 mm wide in the middle, 4 mm thick, and an I-WP cell type porous specimen. As there is currently no specific standard for testing the compressive properties of 3D-printed porous bone scaffolds, the test method was modified in ASTM D695,[22,23] and the compressive specimen was a 9 × 9 × 9 mm porous cube. The two constructed models are shown in Fig. 1.

2.2 Materials

PCL powder (Capa 6400; Perstorp, the molecular weight of about 50 000; melting point 60 °C) was purchased from Chuangjin Plastics Co., Ltd; CSH (CAS: 10034-76-1) was purchased from Guangdong Mingtu Chemical Co., Ltd; phosphate buffer-sterile (PBS, 0.1 M, pH = 7.4) and modified-simulated body fluid (SBF, Cat No.: PH1820, pH = 7.4) were purchased from Fuzhou Feijing Biotechnology Co., Ltd.

2.3 Preparation of composite powder and scaffold

The preparation process of the composite scaffold, as shown in Fig. 1(a), involves two main stages: composite powder preparation and selective laser sintering (SLS) specimen fabrication.

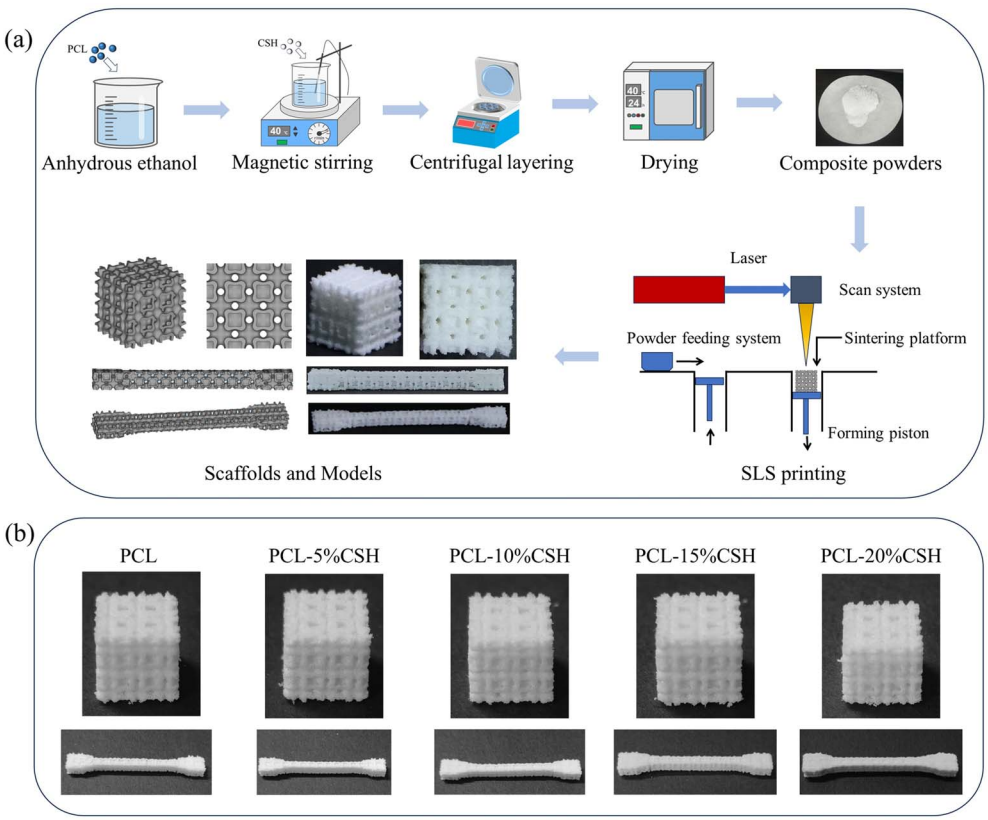

Fig. 1 Flow chart of scaffolds and powders preparation. (a) Preparation flow chart; (b) morphology of the prepared scaffold.

2.3.1 Preparation of composite powders. PCL/CSH composite powders with CSH contents of 0, 5, 10, 15, and 20 wt% were prepared. (i) After weighing the corresponding proportion of powder, the PCL powder was first poured into a beaker containing anhydrous ethanol and stirred at 40 °C for 45 min using a constant temperature magnetic stirrer (DF-101S, Shanghai Qiuzuo Scientific Instrument Co., Ltd) to evenly disperse the powder in the beaker. Then pour the corresponding proportion of CSH into the beaker and stir for 45 minutes to make the composite powder fully mixed. (ii) The suspended turbid liquid was transferred to a high-speed centrifuge (SN-LSC-40, Shangpu Instrument Equipment Co., Ltd, Shanghai, China) and centrifuged at 600 rpm for 10 min to collect the wet powder. (iii) The powder was placed in a drying oven (101-3AS, Beijing Yongheng Guangming Medical Instrument Co., Ltd) and dried at a constant temperature of 40 °C. Its weight was measured every 24 hours until that a constant weight was reached. (iv) Remove the powder and grind it repeatedly until it passes through a 100-mesh sieve.

2.3.2 SLS preparation of specimens. The designed scaffold model was prepared using the SLS, with the laser scanning speed controlled to 900 mm s^{-1}, the spacing to 0.15 mm, the path cross-filling, the power to 6 W, and the sintered single layer thickness to 150 μm.

The molding outcomes of all scaffolds with different CSH contents are shown in Fig. 1(b), exhibiting a complete and intact structure.

2.4 Characterization

The micromorphology of the scaffolds and powders was analyzed using a scanning electron microscope (SEM, Phenom ProX, Phenom-World BV, Eindhoven, Netherlands). The phase composition of CSH and PCL/CSH composite scaffolds was analyzed using X-ray diffraction (XRD, AL2700B, Dandong Aolong Ray Instrument Co., Ltd, China). The composite scaffolds were measured and analyzed using a Fourier transform infrared spectrometer (FTIR, NicoletteTM 6700, Thermo Scientific IN10, USA). The porosity of the scaffolds was measured before and after immersion. The porosity of the scaffolds was measured using the pycnometer method based on the Archimedean principle using anhydrous ethanol as the liquid medium, which was obtained by the following formula.

$$P(\%) = \frac{W_2 - W_3 - W_4}{W_1 - W_3} \quad (1)$$

Among them, W_1 is the weight of the bottle filled with anhydrous ethanol; W_2 and W_3 are the weights of the bottle after being placed in and taken out of the rack (filled with anhydrous ethanol), respectively; W_4 is the dry weight of the rack in air.

2.5 Mechanical properties

A universal testing machine (Dongguan ZQ-990LA) was used to conduct uniaxial tensile and compressive tests on the scaffolds. The tensile/compressive speed was 1 mm min^{-1} and the load was 1 kN. The experimental equipment automatically recorded the test results of each experiment.

In order to measure the self-setting effect of the scaffold, the scaffold was placed in a sealed bag of distilled water and gently squeezed to accelerate the infiltration of water molecules. The CSH self-setting was basically in a stable state after two hours.[24] After two hours, the scaffold was taken out and placed in a drying oven at a temperature of 40 °C to dry. Its weight was measured every 24 hours until it was constant. The dry and wet scaffold mechanics were measured after two hours of immersion.

2.6 Water contact angle measurement

Use a dropper to drop 5 μl of red pigment ink vertically on the sample and use a digital camera to record the morphology of the water droplet in the first second and calculate the water contact angle.[25]

2.7 Degradation performance

The water absorption is determined by measuring the weight gain of the specimen after soaking in a distilled water solution for 2 hours. The determination is made by weighing the specimen and then soaking it in distilled water for the specified duration. At the predetermined time, the specimen is removed from the solution, the surface water is wiped off, and the weight of the specimen is then measured. The formula for calculating the water absorption rate of the specimen:

$$\text{Water absorption}(\%) = \frac{m_1 - m_0}{m_0} \times 100\% \quad (2)$$

Among them, m_0 is the initial weight, and m_1 is the weight after two hours of soaking in distilled water.

The degradation performance of the composite scaffolds was evaluated by soaking in PBS solution. Each group of scaffolds was placed in a centrifuge tube filled with PBS solution and then placed in a 37 °C incubator. The solution was changed every 7 days. The scaffolds were taken out on the 7th, 14th, 21st, and 28th days (no less than 3 times for each group), washed repeatedly with anhydrous ethanol, dried in a 40 °C constant-temperature drying oven, and weighed every 24 hours until a constant weight was achieved. The weight was measured, the weight loss was calculated, and the surface morphology was observed by SEM to study the effect of CSH content on the degradation of the scaffold. In addition, the mechanical properties of the scaffolds were measured on the 7th and 14th days of immersion. The relationship between degradation and mechanics was preliminarily evaluated. The weight loss rate of the sample was calculated as follows:

$$\text{Weight loss}(\%) = \frac{m_2 - m_0}{m_0} \times 100\% \quad (3)$$

Among these, m_0 represents the initial weight, while m_2 denotes the dry weight after soaking in PBS.

In addition, in order to measure the changes in pH, the cumulative pH value of each group of solutions was measured on the 2, 4, 6, 8, and 10 days without changing the PBS solution.

2.8 Biomineralization ability

Soaking the composite scaffolds in SBF solution assessed their capacity for biomineralization. The scaffold was placed in a centrifuge tube containing SBF solution and then placed in a 37 °C incubator, with the solution changed every 2 days. On the 7th day, the scaffold was removed, its surface was cleaned with anhydrous ethanol, and it was then dried in a 40 °C drying oven. The scaffold was weighed every 24 hours until a constant weight was reached. The surface morphology of the scaffold was examined using SEM, and XRD analyzed its phase composition.

2.9 Statistical analysis

Quantitative data were analyzed statistically in this study. Data are presented as the mean ± standard deviation (SD). Group differences were assessed using one-way analysis of variance (ANOVA), with a $p < 0.05$ considered statistically significant. Groups that do not share the same letters (*e.g.*, a, b, c) are significantly different from each other.

3. Results and discussion

3.1 Phase composition analysis

The morphological characteristics of PCL and CSH powders are shown in Fig. 2(a and b), and their shapes are irregular. Fig. 2(c) is a histogram of PCL particle size distribution. It can be seen that the particle size of PCL particles is mainly concentrated in 60–100 μm, with a peak at about 80 μm. A small number of particles have a particle size of more than 200 μm, indicating that the particle size distribution of PCL particles is relatively wide. Fig. 2(d) shows the particle size distribution of CSH particles, showing that the particle size of CSH particles is mainly concentrated in 1–2 μm, with a peak at 1 μm. The particle size distribution is relatively narrow, and almost all

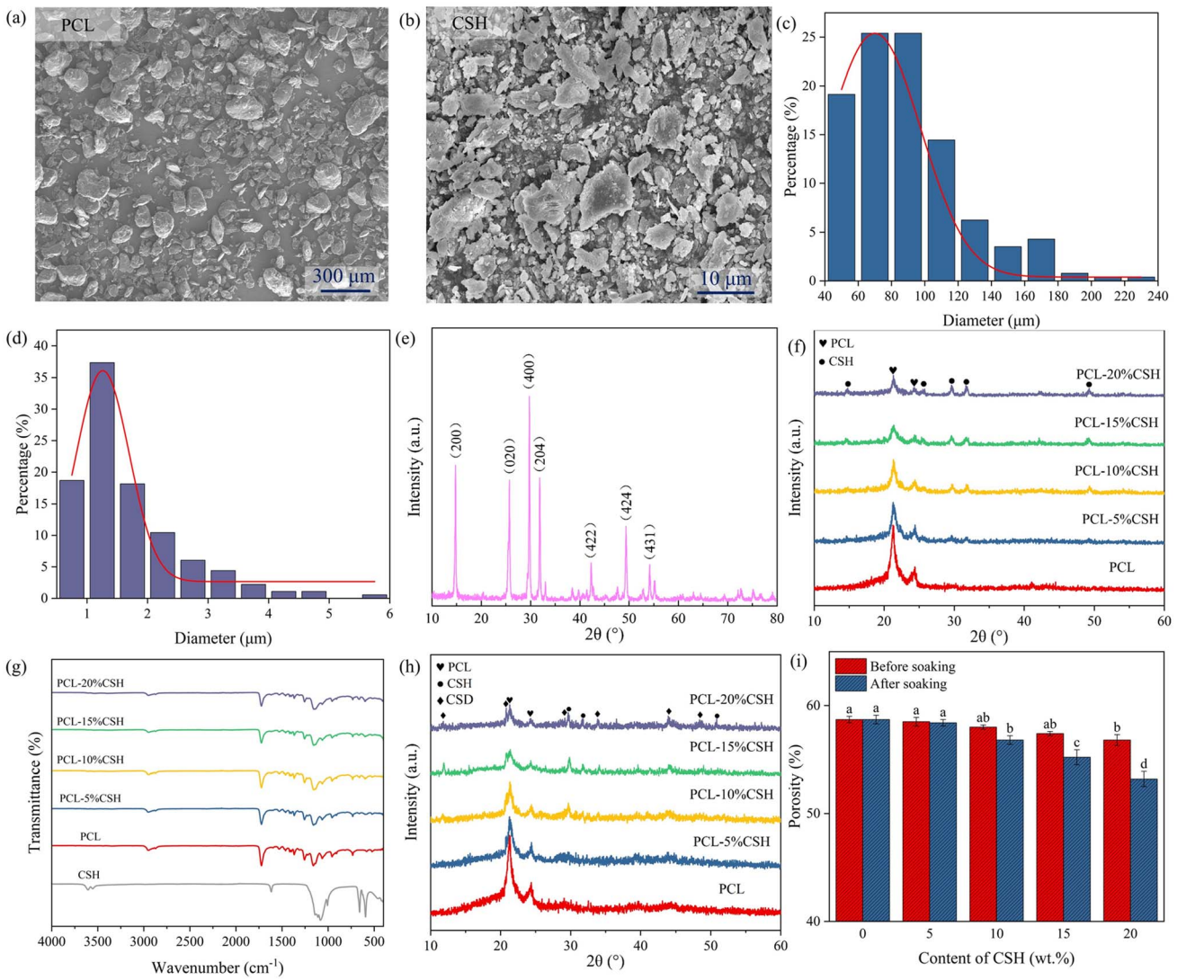

Fig. 2 Characterization of powders and scaffolds. (a) SEM image of PCL; (b) SEM image of CSH; (c) PCL particle size distribution; (d) CSH particle size distribution; (e) XRD pattern of CSH; (f) XRD patterns of the scaffolds. (g) FTIR spectra of CSH and scaffolds. (h) XRD patterns of the scaffolds after soaking. (i) Porosity of the scaffold before and after soaking.

particles are less than 5 μm. As shown in Fig. 2(e), the XRD pattern of CSH shows that its main characteristic diffraction peaks are at 14.7°, 25.7°, 29.7°, 31.8°, and 49.3°.[16] The XRD patterns of the five groups of sintered composite scaffolds are shown in Fig. 2(f). PCL has main characteristic diffraction peaks at 21.3° and 24.3°. With the increase of CSH content, the diffraction peak area of PCL gradually decreases, and the addition of CSH reduces the crystallinity of PCL. In addition, the main characteristic diffraction peak of CSH in the composite scaffold is strengthened, while the main characteristic diffraction peak intensity of PCL gradually decreases. CSH maintains its stable hydration structure during the sintering process, and no other impurity peaks are generated during the sintering process of the scaffold. The functional group structure

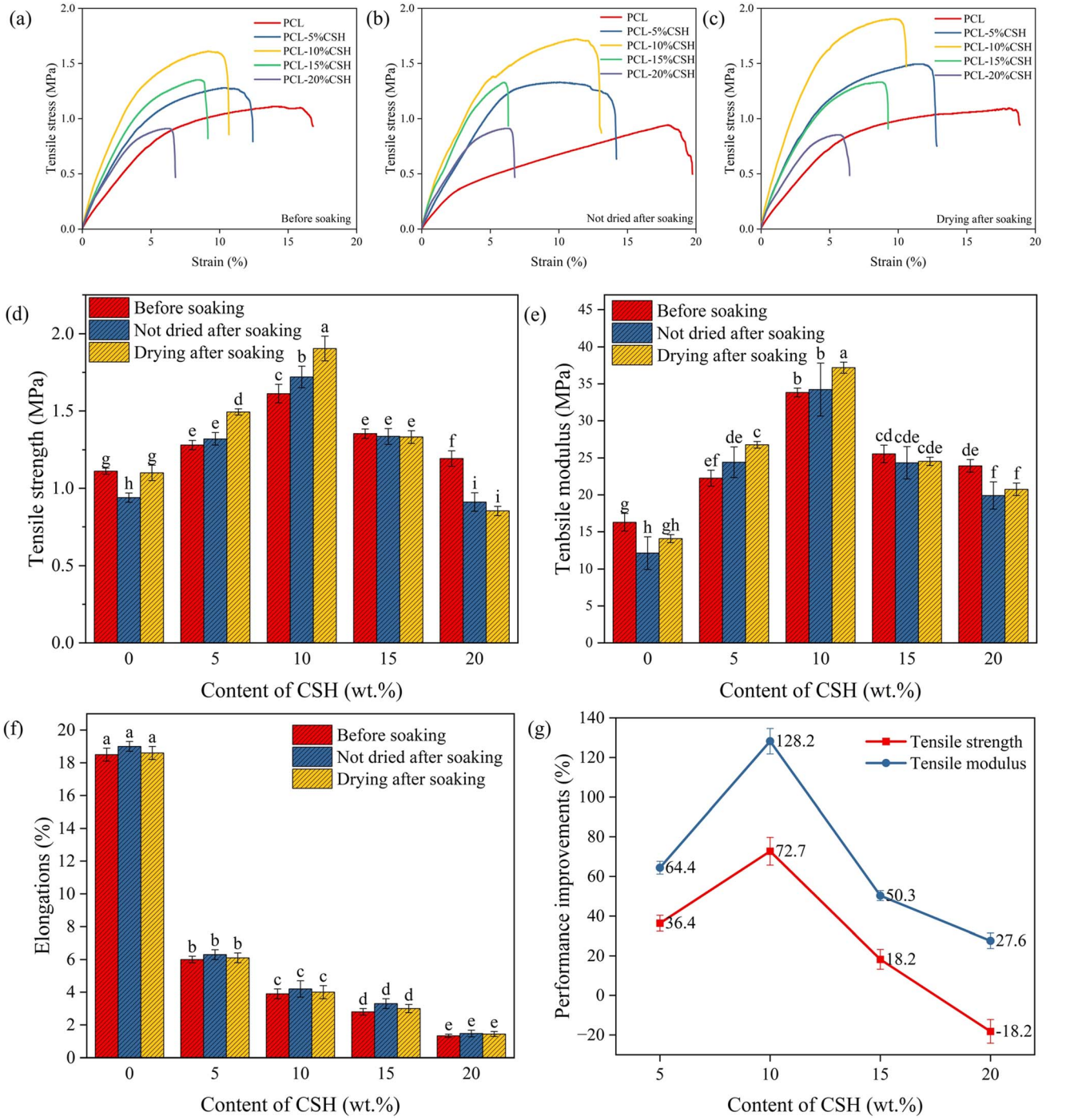

Fig. 3 Tensile properties of different scaffolds. Stress–strain curves of (a) before soaking and (b) not dried after soaking and (c) drying after soaking; (d) strength; (e) modulus; (f) elongation; (g) performance improvement.

of PCL/CSH composites was analyzed by FTIR. As shown in Fig. 2(g), CSH powder has a strong broad band of S–O at 1141 cm^{-1} and secondary bands at 661 cm^{-1} and 592 cm^{-1} caused by SO_4^{2-}. The peak of CSH was observed in the composite, and its peak intensity increased with the content. No new characteristic peaks appeared after the composite of PCL and CSH, and no significant shift of the main absorption peaks of PCL or CSH was observed. In addition, the XRD patterns of the five groups of proportional scaffolds after being soaked in distilled water for two hours are shown in Fig. 2(h). Different from before soaking, the main characteristic diffraction peaks of calcium sulfate dihydrate (CSD) were detected at 11.7°, 20.8°, 29.2°, and 33.8°, indicating that CSH was underwent self-setting and successfully transformed into CSD.[26,27] Finally, the porosity before and after immersion was measured. As shown in Fig. 2(i), the experimental results show that the porosity of the scaffold gradually decreases with the content of CSH after immersion, which is closely related to the hydration reaction of CSH. On the one hand, during the immersion process, CSH absorbs water and undergoes hydration reaction, converting into CSD. This conversion may cause the volume expansion inside the material, partially filling the original pores, thereby reducing the overall porosity. On the other hand, during the formation of CSD, some newly generated crystals are deposited on the pore surface inside the scaffold, causing the pores to partially close or shrink, resulting in a decrease in the overall porosity. The reaction equation for the conversion of CSH to CSD is:

$$CaSO_4 \cdot 0.5H_2O + 1.5H_2O \rightarrow CaSO_4 \cdot 2H_2O + \text{heat} \quad (4)$$

3.2 Mechanical properties

As shown in Fig. 3(a–e), whether before or after soaking, as the CSH content increases, the tensile strength and modulus of the composite scaffolds first increase and then decrease, reaching a maximum value at 10 wt%. When the CSH content was 10 wt%, before soaking, the tensile strength and modulus of the composite scaffold were 1.6 MPa and 33.8 MPa, respectively, which were 45.5% and 107.4% higher than those of the pure PCL (tensile strength: 1.1 MPa, tensile modulus: 16.3 MPa) scaffold; after drying, it's tensile strength and modulus were 1.9 MPa and 37.2 MPa, which were 72.7% and 128.2% higher than those of pure PCL scaffold. As a hard inorganic component, CSH can improve the stiffness and strength of the composites through interaction with polycaprolactone. When the CSH content exceeded 10 wt%, the composite scaffold did not show the self-setting enhanced mechanical effect. It is worth noting that the mechanical comparison of the dry and wet scaffolds after immersion for 2 hours found that the tensile modulus increased after drying, which may be related to the fact that the self-setting reaction of CSH in the wet scaffold was still ongoing; when the CSH content exceeded 10 wt%, the tensile strength after drying decreased, which was due to the fixation of the CSD morphology after drying and further expansion of the cracks. As shown in Fig. 3(f), with increasing CSH content, the elongation at the break of the scaffold gradually decreased, and the elongation at the break before and after soaking remained almost unchanged. The improvement in performance of the five groups of composite scaffolds relative to the PCL scaffolds after drying are shown in Fig. 3(g). It can be seen that when the CSH content is 10 wt%, the tensile properties after self-setting are optimal.

The compressive stress–strain of the five groups of proportional scaffolds is shown in Fig. 4(a–e). Since PCL is a plastic material, the scaffold did not break during the compressive process. When the strain exceeded 40%, it was almost impossible for the scaffold to recover its original shape and pore structure after being deformed by force. Therefore, 40% strain was taken as a unified standard to evaluate each composite scaffold's compressive strength and modulus. Regardless of before or after soaking, as the CSH content increases, the compressive strength and modulus of the scaffold also show a trend of first increasing and then decreasing, and both reach the maximum value at 10 wt%. When the CSH content was 10 wt%, the compressive strength and modulus of the composite scaffold were 3.5 MPa and 16.3 MPa, respectively, which were 40.0% and 39.3% higher than those of the PCL scaffold (compressive strength: 2.5 MPa, compression modulus: 11.7 MPa). After soaking and drying, the compressive strength and modulus of the composite scaffold were 4.2 MPa and 19.2 MPa, respectively, which were 68.0% and 64.1% higher than those of the PCL scaffold. In addition, by comparing the wet and dry scaffolds after immersion, it can be seen that the modulus of the dried scaffolds are improved, but when the CSH content exceeds 10 wt%, the strength are reduced. It can be seen that when the CSH content is 10 wt%, the mechanical enhancement effect is optimal.

3.3 SEM characterization

The surface microstructures of the five groups of proportional scaffolds before and after soaking were characterized by SEM observation, as shown in Fig. 5. Before soaking, the surface of the PCL scaffold was relatively smooth, and the CSH particles on the surfaces of PCL-5% CSH and PCL-10% CSH scaffolds were evenly distributed; when the CSH content exceeded 10 wt%, the CSH particles showed small-scale agglomeration, which may also be the main reason why the compressive strength of the composite scaffold first increases and then decreases. When CSH is evenly dispersed and filled into PCL, it can improve the stiffness of the scaffold and effectively share the external compressive load of the scaffold.[28] However, when CSH agglomerates within the PCL matrix, defects and stress concentration points are easily formed, ultimately causing a reduction in the material's mechanical properties. The formation of these agglomerates can be attributed to interactions between chemical bonds, van der Waals forces, and Coulomb forces.[29]

After soaking, the surface of the PCL scaffold did not change, composite scaffolds showed a large number of columnar crystals overflowing on the scaffold surface, and they gradually increased with the increase of CSH content. This was the result of CSH self-setting and conversion to CSD. When the CSH content is less than 10 wt%, the columnar crystals formed on

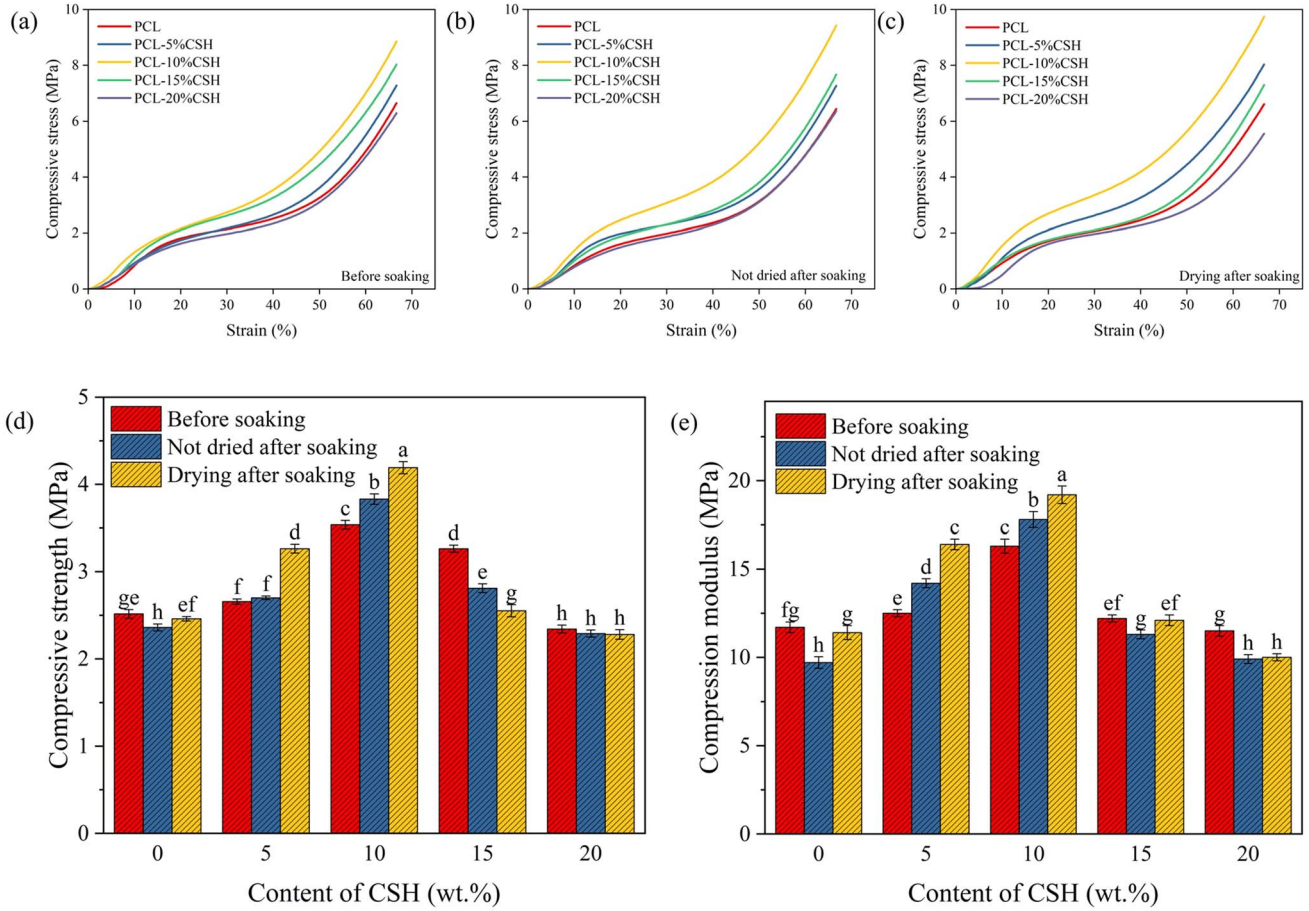

Fig. 4 Compression properties of the different scaffolds at 40% strain. Stress–strain curves of (a) before soaking and (b) not dried after soaking and (c) drying after soaking; (d) strength; (e) modulus.

the surface may partially fill the pores of the scaffold, leading to a decrease in the scaffold's porosity and an increase in its compressive strength. However, it is noteworthy that defects appeared in PCL-15% CSH and PCL-20% CSH scaffolds, which were associated with the agglomeration of CSH before soaking. After self-setting, the defects increase and the stress

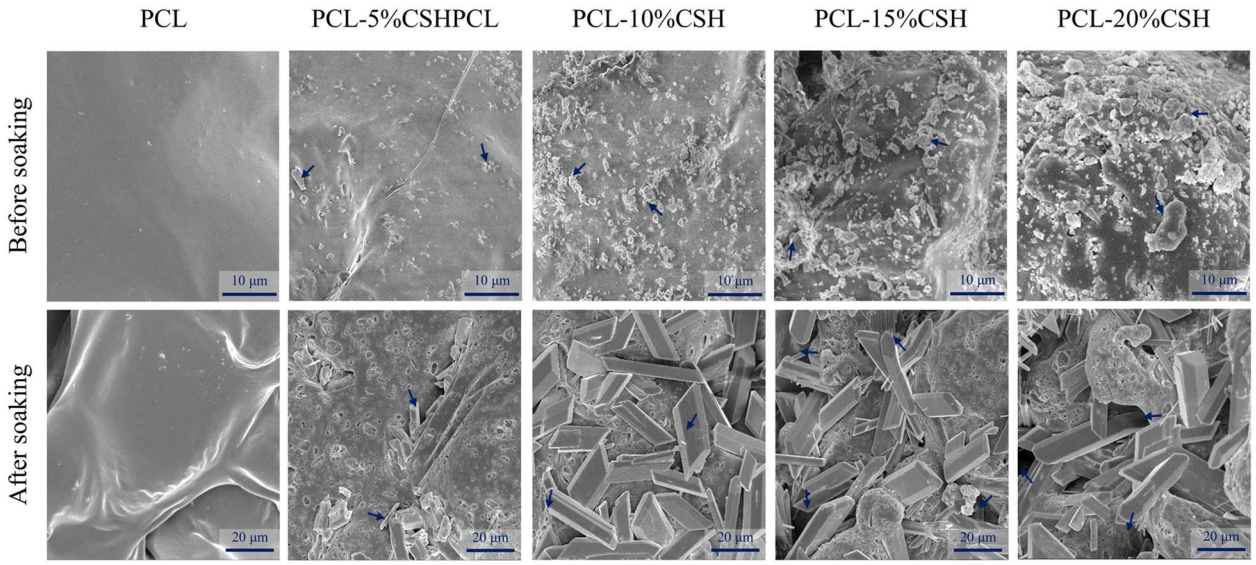

Fig. 5 Microscopic surface morphology of different scaffolds.

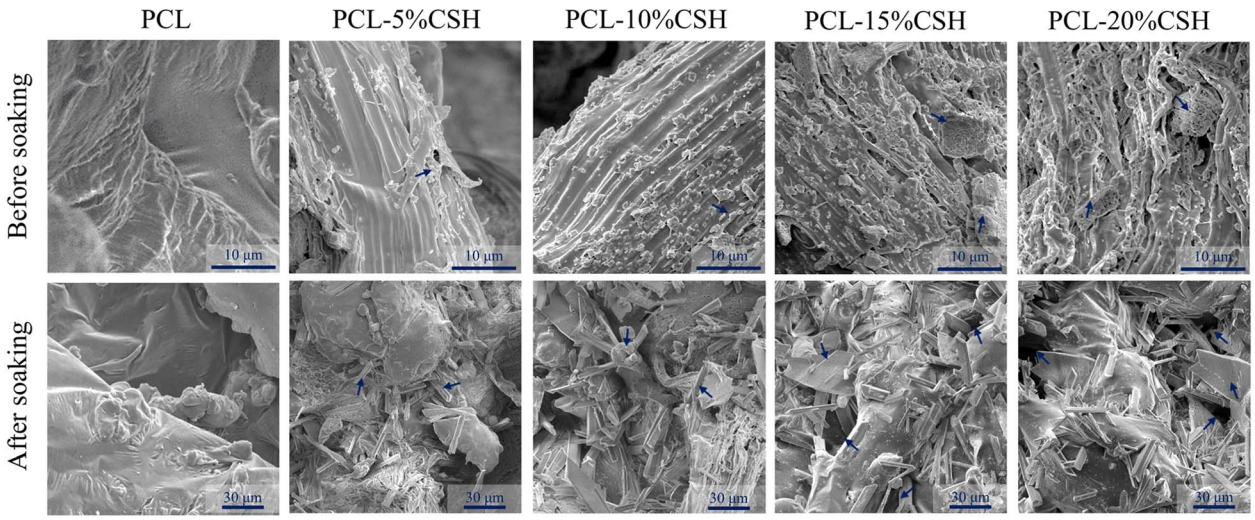

Fig. 6 Tensile fracture morphology of different scaffolds.

concentration intensifies, which leads to a decrease in the compressive strength of the scaffold after soaking.

The SEM images of the tensile fracture of the composite scaffold before and after soaking are shown in Fig. 6. Before soaking, when the CSH content does not exceed 10 wt%, it can be evenly filled into the PCL matrix as a small particle filler, which can limit the slippage of the polymer chain to a certain extent, thereby improving the tensile strength. When the content exceeds 10 wt%, CSH particles agglomerate on a small scale, resulting in uneven force. In addition, the high content of CSH makes the composite material more fragile, and its ductility and toughness are significantly reduced as shown in Fig. 3(e), causing the composite scaffold's tensile strength to decline.

After soaking, the tensile fracture surface showed many columnar crystals interspersed and embedded in the PCL matrix, indicating that after the composite scaffold was self-setting, the newly grown columnar crystals effectively produced a pinning effect on the PCL. Therefore, the tensile strength of the composite scaffold is enhanced. When the CSH content exceeds 10 wt%, many defects appear on the fracture

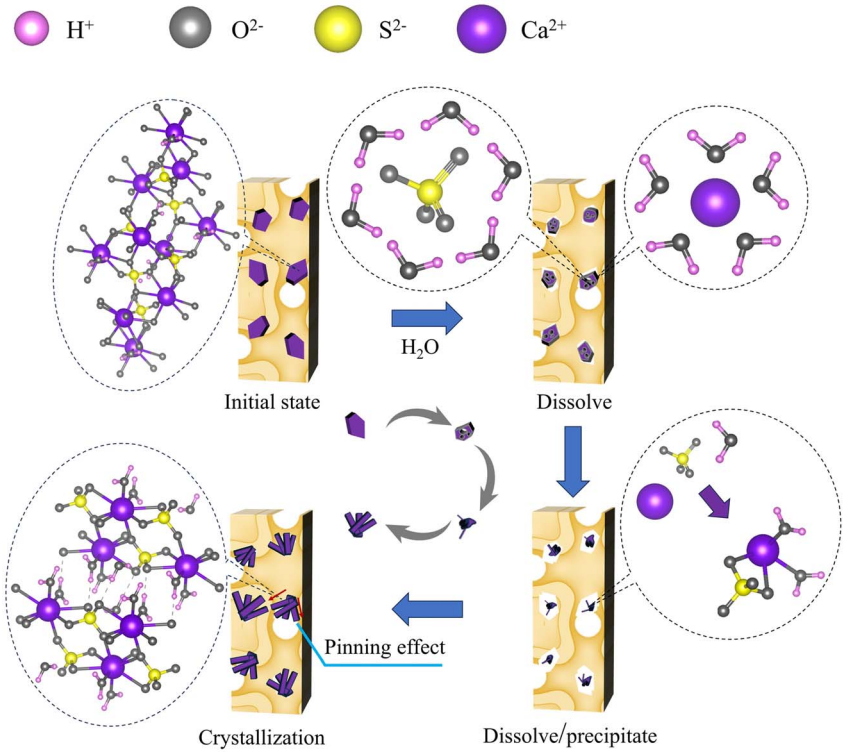

Fig. 7 Self-setting enhancement mechanical mechanism.

surface of the composite scaffold. It can be seen that the agglomerated CSH is transformed into CSD; that is, after self-setting, it is easy to form larger defects, aggravating the original stress concentration and thereby reducing the tensile strength of the composite scaffold. The appearance of a small number of plate-like crystals may be related to the heat release caused by the self-setting of CSH, which leads to an increase in local temperature and affects the growth direction of some crystals.[26]

3.4 Self-setting strengthening mechanical mechanism

As shown in Fig. 7, the self-setting process of CSH is a concurrent dissolution/precipitation process, which can be roughly divided into three stages.

3.4.1 Stage 1: dissolution. Water molecules have strong hydrogen bonds. When CSH comes into contact with water molecules, the electrostatic force between ions destroys the original water structure and forms a water layer around the ions. According to La Bella *et al.*, the (010) and (100) surfaces of CSH have higher solid–water interfacial energy and stronger interaction with water. This interaction causes the middle part of CSH to be more easily dissolved first in an aqueous environment.[24,27]

3.4.2 Stage 2: dissolution/precipitation. As water molecules gradually penetrate the scaffold, CSH dissolves faster. Since the solubility of CSD in water is much lower than that of CSH, when the Ca^{2+} and SO_4^{2-} ions in the solution reach saturation and exceed the solubility of CSD, they will recombine to form CSD and precipitate.

3.4.3 Stage 3: crystallization. As time goes by, the CSH particles gradually disappear, and the CSD gradually precipitates and grows. Finally, under the influence of the environment, columnar or plate-like crystals with high crystallinity grow in different directions.[30]

During the whole process, when the CSD morphology is stable and the hardness remains unchanged, the self-setting reaction is basically completed. When CSH transforms into CSD crystals, these crystals gradually grow within the PCL matrix and are finally embedded in the PCL molecular chains. At this time, the pinning effect of CSD on PCL limits the free movement of PCL molecular chains, thereby enhancing the mechanical properties of the composite scaffold.[31,32]

3.5 Degradation performance

The favorable hydrophilicity of the scaffold promotes the penetration of water molecules into the interior of the scaffold, thereby accelerating the self-setting of CSH and the degradation

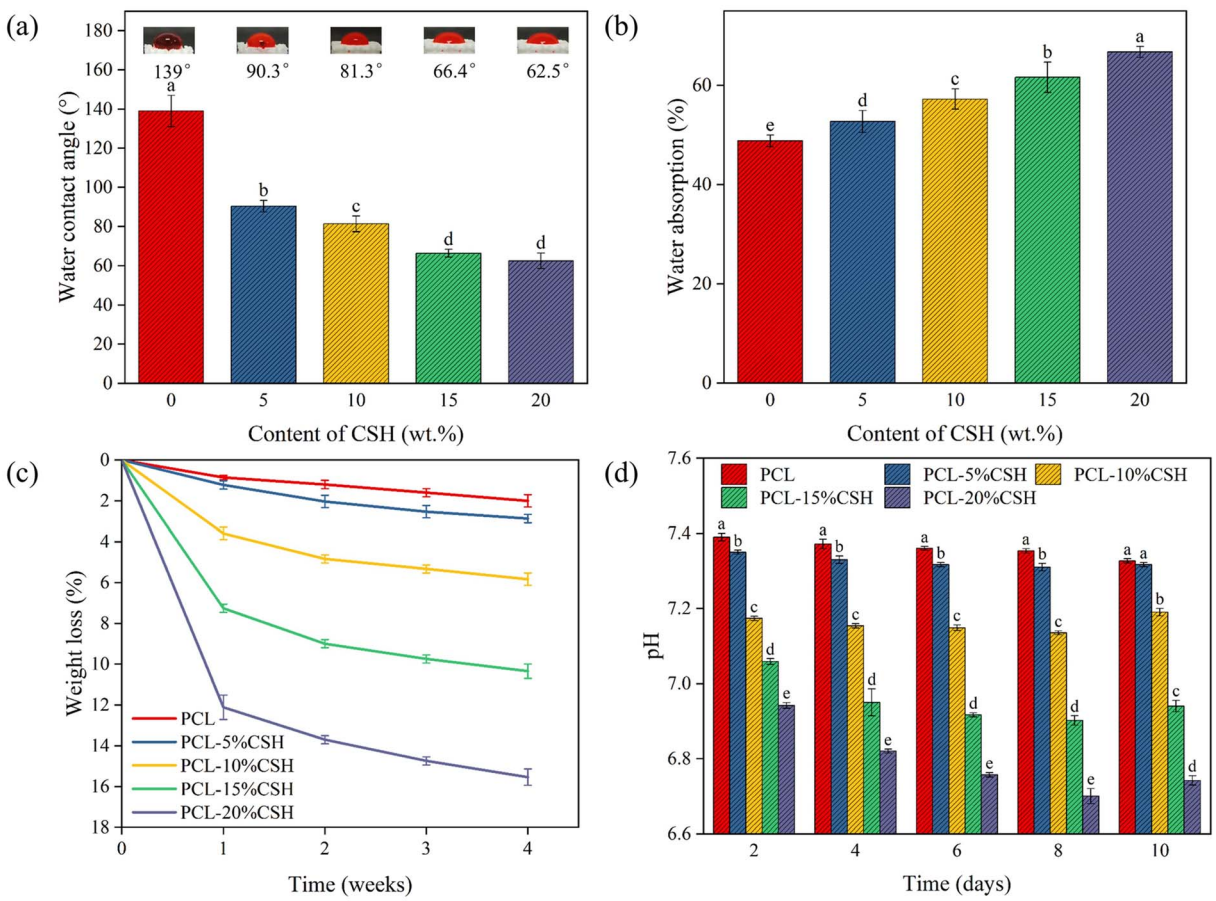

Fig. 8 Changes in degradation properties of different scaffolds. (a) Water contact angle; (b) water absorption; (c) weight loss of the scaffolds; (d) pH of the solution.

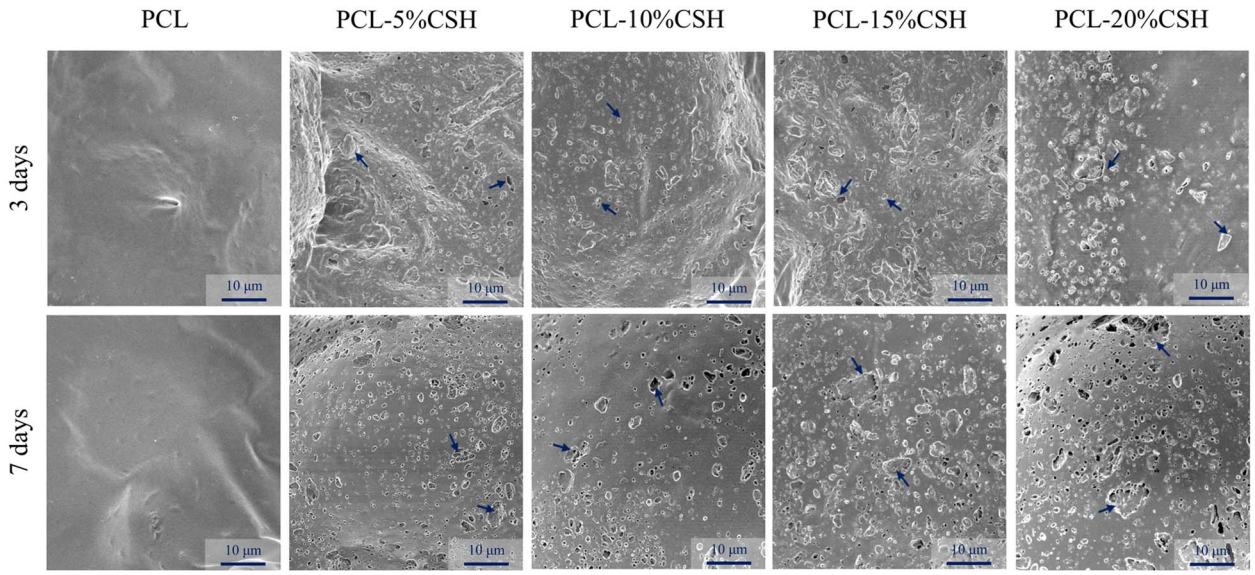

Fig. 9 Microscopic morphologies of different scaffolds after soaking in PBS.

of the scaffold. As shown in Fig. 8(a), the water contact angle of the PCL scaffold is 139°, which is hydrophobic. As the CSH content increases, the water contact angle gradually decreases, and the PCL-20% CSH scaffold reaches the minimum value with a water contact angle of 62.5°. Meanwhile, as shown in Fig. 8(b), the water absorption rate of the scaffold gradually increases with the CSH content. These results indicate that the hydrophilicity of the composite scaffold is significantly enhanced.

Fig. 8(c) shows the weight loss of five groups of scaffolds with different CSH ratios after soaking in PBS solution for 4 weeks. The weight loss of the scaffold is directly proportional to the soaking time and increases gradually with the rise in CSH content. After the scaffold was soaked in PBS solution for 4 weeks, the weight loss of the PCL scaffold was 2%, while the weight loss of the PCL-20% CSH scaffold reached an astonishing 15.5%, about 8 times that of PCL. The degradation rate of the composite scaffold was significantly increased.

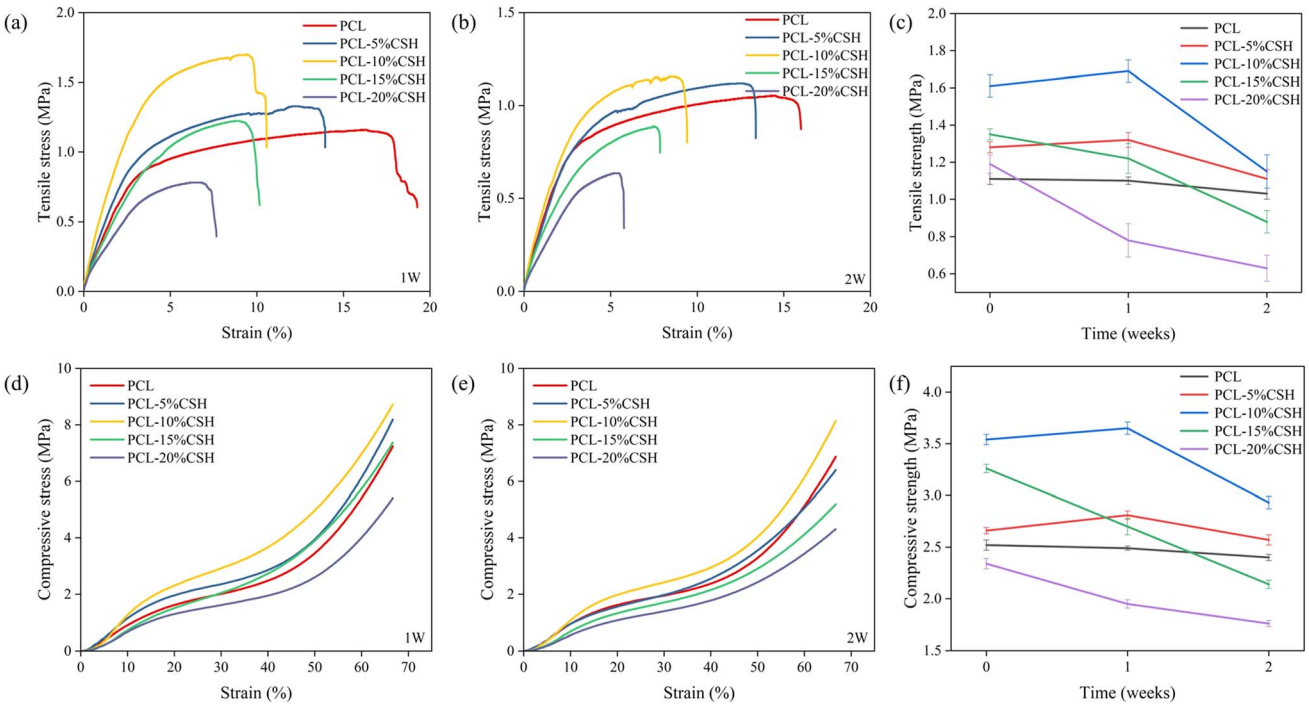

Fig. 10 Changes in soaking time and mechanical properties of different scaffolds. (a) Tensile stress–strain curve after soaking for 1 week and (b) soaking for 2 weeks; (c) tensile strength change; (d) compressive stress–strain curve after soaking for 1 week and (e) soaking for 2 weeks; (f) compressive strength change.

In addition, without changing the PBS solution, the changes in pH values of the scaffolds in the five groups after being soaked in the PBS solution for 10 days are shown in Fig. 8(d). Eight days before PBS soaking, the pH values of all composite scaffold solutions showed a downward trend, especially as the CSH content increased, and the pH values dropped significantly. The PCL-20% CSH scaffold reached the lowest level on the 8th day, approximately 6.7. The pH value of the PCL scaffold was about 7.3 on the 8th day after soaking in PBS, and it showed a continuous decreasing trend for 10 days. The pH value of the PCL-5% CSH scaffold solution slowed down after being soaked in the solution for 8 days, while the pH value of the composite scaffold with a CSH content of 10 wt% and above began to rise after being soaked in PBS for 10 days.

PCL undergoes degradation in both acidic and alkaline environments.[33] Initially, when the scaffold is soaked in PBS solution, the CSH on the surface dissolved and quickly converted into CSD, which degraded to acidity,[34] exceeding the buffering capacity of the PBS solution, and causing the pH value to drop sharply. The acidic conditions formed enable PCL autocatalytic degradation.[35,36] The above studies indicate that the increase in weight loss can be attributed to the increased water absorption, the rapid degradation of CSD, and the autocatalytic degradation of PCL in an acidic environment. The pH value tends to rise after the 8th day, this is because after a large amount of CSD on the surface has been degraded, the overall degradation trend of the composite scaffold has slowed down. At this time, the buffering capacity of the PBS solution plays a role.

The microscopic morphologies of the degradation of five groups of scaffolds with different CSH ratios after soaking in PBS solution for 7 days are shown in Fig. 9. No obvious holes were found on the surface of the PCL scaffold within 7 days, while obvious holes appeared on the surfaces of other composite scaffolds, and the higher the CSH content, the more obvious the holes. On the 3rd day, CSH on the surface of the composite scaffold was converted into CSD and partially dissolved, creating holes. On the 7th day, these holes became more and more obvious, especially in PCL-20% CSH, where large areas of holes appeared and the particles were almost difficult to observe on the surface. Such large areas of holes are caused by the rapid degradation of CSD. The increase in the number of pores facilitates the penetration of the solution into the interior of the composite scaffold, thereby accelerating the degradation of the scaffold. This phenomenon is responsible for the notable reduction in the composite scaffold's weight and the pH value of the PBS solution.[37]

Finally, a preliminary evaluation was conducted on the relationship between the degradation and mechanical properties of the scaffolds. As shown in Fig. 10(a–f), the mechanical properties

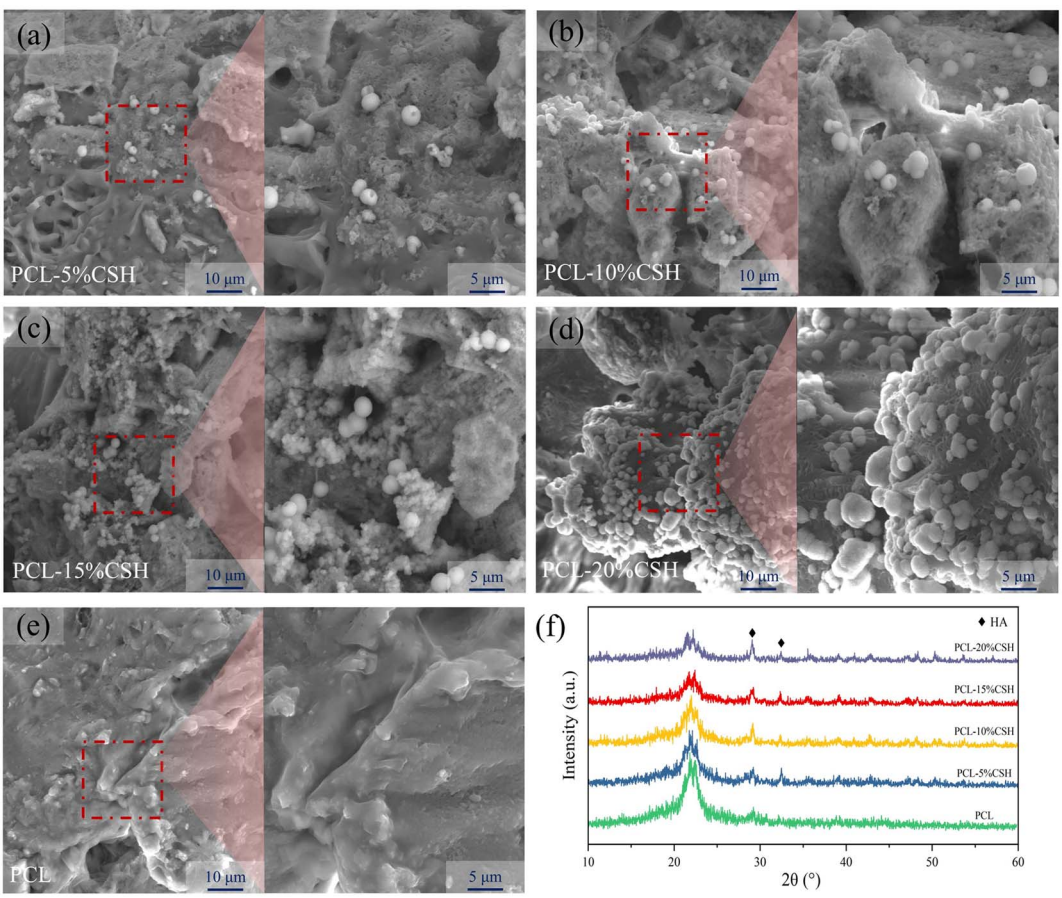

Fig. 11 Surface micromorphology and XRD patterns of the scaffolds after soaking in SBF for 7 days. (a) PCL-5% CSH, (b) PCL-10% CSH, (c) PCL-15% CSH, (d) PCL-20% CSH, and (e) PCL represent the microscopic morphologies of the scaffolds. (f) XRD patterns of the scaffolds.

of PCL-5% CSH and PCL-10% CSH scaffolds were improved after being immersed in PBS solution for one week. This is due to the pinning effect of the internal CSH self-setting on the PCL, which resulted in a significant improvement in the mechanical properties. The mechanical properties of PCL-15% CSH and PCL-20% CSH scaffolds declined because the self-setting of the originally agglomerated CSH aggravated the stress concentration. Secondly, the weight loss of the composite scaffold was too large and the internal structure was incomplete, resulting in reduced mechanical properties. In the second week, due to the continuous penetration of the solution into the scaffold, the CSD inside gradually degraded, causing the internal structure to lose its original integrity, resulting in a decrease in the mechanical properties of all composite scaffolds.[38]

3.6 *In vitro* bioactivity assessment

The composite scaffold's good hydroxyapatite (HA) forming ability is key to the material's ability to induce osteogenesis.[39] The biomineralization ability of the composite scaffolds was evaluated by soaking in SBF. Fig. 11(a–e) shows the SEM morphologies of the scaffolds with five groups of CSH contents after being soaked in SBF for 7 days. As the CSH content increased, the spherical deposits formed on the surface of the composite scaffold gradually increased, and the deposits on the PCL-20% CSH scaffold were the most obvious; in contrast, no deposit formation was observed on pure PCL. Phase analysis of the composite scaffolds using XRD is shown in Fig. 11(f). Significant peaks of hydroxyapatite were detected at 29° and 32.5°, further proving that the surface deposits are HA.[40–42] This phenomenon is due to the conversion of CSH into CSD in the solution, which then degrades and releases a large amount of Ca^{2+} ions, which combine with PO_4^{3-} ions in the solution to form amorphous calcium phosphate and attach to the surface of the scaffold. The results of the above experiments demonstrate that the composite scaffold effectively induces hydroxyapatite formation.

4. Conclusion

Herein, a porous PCL/CSH composite scaffold with self-setting properties was prepared through a triply periodic minimal surfaces (TPMS) design and selective laser sintering (SLS) technology. The main findings and conclusions are as follows:

(1) The self-setting mechanical enhancement of the scaffold originates from the fact that CSH is transformed into columnar crystals, which are interspersed and embedded in the PCL molecular chains, reshaping the interface bonding with PCL. The PCL-10% CSH scaffold exhibits the best compressive and tensile strengths, which are increased to about 1.7 times that of the PCL scaffold.

(2) CSH acts as a catalyst to accelerate the degradation of the scaffold. Its main functions are: (i) the pores produced by the high-speed degradation are conducive to the penetration of the solution into the interior of the scaffold, accelerating the degradation of the scaffold; (ii) CSH creates a local acidic environment during the dissolution and transformation of CSD and the degradation of CSD, thereby catalyzing the degradation of PCL.

(3) After soaking in SBF solution for 7 days, a large amount of spherical apatite was deposited on the surface of the composite scaffold, showing good bioactivity.

In summary, this PCL/CSH scaffold with self-setting properties provides a new idea for bone defect repair.

Data availability

The data supporting the findings of this study were collected during the completion of an academic paper and are currently stored on a personal computer. Due to data protection, they are not available in a public repository. However, the data may be accessed upon reasonable request. Contact Angela Patricia Sanchez Cepeda *via* email to sciencefield@126.com.

Conflicts of interest

The authors declare that they have no known competing financial interests or personal relationships that could have appeared to influence the work reported in this paper.

Acknowledgements

This work was supported by the following funds: (1) Scientific Research Foundation of Hunan Provincial Education Department (24A0535); (2) Natural Science Foundation of Hunan Provincial (2022JJ50182); (3) Graduate Research and Innovation Project of Shaoyang University (CX2023SY063).

References

1 Y. Chen, S. Quan, S. Huang, W. Liu, Z. Chen, J. Liu, C. Li and H. Yang, *Ceram. Int.*, 2024, **50**, 48891–48908.
2 X. Sheng, Z. Che, H. Qiao, C. Qiu, J. Wu, C. Li, C. Tan, J. Li, G. Wang, W. Liu, H. Gao and X. Li, *Int. J. Biol. Macromol.*, 2024, **277**, 133806.
3 L. Li, J. Shi, K. Ma, J. Jin, P. Wang, H. Liang, Y. Cao, X. Wang and Q. Jiang, *J. Adv. Res.*, 2021, **30**, 75–84.
4 S. Kumar Parupelli, S. Saudi, N. Bhattarai and S. Desai, *Int. J. Bioprint.*, 2023, **9**, 0196.
5 X. Zhao, N. Li, Z. Zhang, J. Hong, X. Zhang, Y. Hao, J. Wang, Q. Xie, Y. Zhang, H. Li, M. Liu, P. Zhang, X. Ren and X. Wang, *J. Nanobiotechnol.*, 2024, **22**, 500.
6 E. Bagherzadeh, Z. Sherafat, S. M. Zebarjad, A. Khodaei and S. A. Yavari, *J. Mater. Res. Technol.*, 2023, **23**, 379–390.
7 O. Gil-Castell, J. Badia, I. Ontoria-Oviedo, D. Castellano, P. Sepúlveda and A. Ribes-Greus, *Mater. Sci. Eng. C*, 2020, **107**, 110296.
8 R. S. Azarudeen, M. N. Hassan, M. A. Yassin, M. Thirumarimurugan, N. Muthukumarasamy, D. Velauthapillai and K. Mustafa, *React. Funct. Polym.*, 2020, **146**, 104445.
9 S. Punj, J. Singh and K. Singh, *Ceram. Int.*, 2021, **47**, 28059–28074.

10 I. Alonso-Fernández, H. J. Haugen, M. López-Peña, A. González-Cantalapiedra and F. Muñoz, *Acta Biomater.*, 2023, **168**, 1–21.
11 J. Han, J. Wu, X. Xiang, L. Xie, R. Chen, L. Li, K. Ma, Q. Sun, R. Yang and T. Huang, *Mater. Des.*, 2023, **225**, 111543.
12 C. Paredes, F. J. Martínez-Vázquez, A. Pajares and P. Miranda, *Ceram. Int.*, 2021, **47**, 17726–17735.
13 J. H. Yun, H.-Y. Lee, S. H. Yeou, J. Y. Jang, C.-H. Kim, Y. S. Shin and D. D. D'Lima, *Mater. Today Bio*, 2024, **29**, 101283.
14 A. P. N. Hong, N. T. T. Le, M.-D. Truong, D. L. Tran, N. H. Nguyen and D. H. Nguyen, *Ceram. Int.*, 2024, **50**, 54125–54133.
15 M. Du, Q. Li, J. Chen, K. Liu and C. Song, *Chem. Eng. J.*, 2021, **420**, 129866.
16 W.-Y. Zhou, Y.-B. Zhou, S.-W. Wang, P. Wang and S.-H. Teng, *Ceram. Int.*, 2021, **47**, 23814–23820.
17 A. La Gatta, A. De Rosa, P. Laurienzo, M. Malinconico, M. De Rosa and C. Schiraldi, *Macromol. Biosci.*, 2005, **5**, 1108–1117.
18 J. Ma, Y. Li, Y. Mi, Q. Gong, P. Zhang, B. Meng, J. Wang, J. Wang and Y. Fan, *J. Tissue Eng.*, 2024, **15**, 20417314241263689.
19 Y. Xu, W. Ding, M. Chen, X. Guo, P. Li and M. Li, *Mater. Des.*, 2023, **231**, 112026.
20 D. Li, H. Du, W. Guo, M. Chen, X. Guo, P. Li, Y. Zhou, P. Chen, M. Li and Y. Xu, *RSC Adv.*, 2023, **13**, 24519–24535.
21 S. Q. Zhu, J. J. Lu, M. X. Fan, Y. Chernysh, Y. J. Pan, R. Q. Dang, J. P. Guan, L. C. Yu, B. C. Lin and X. J. Shen, *Polym. Compos.*, 2023, **45**, 4338–4347.
22 F. Guo, E. Wang, Y. Yang, Y. Mao, C. Liu, W. Bu, P. Li, L. Zhao, Q. Jin, B. Liu, S. Wang, H. You, Y. Long, N. Zhou and W. Guo, *Int. J. Biol. Macromol.*, 2023, **242**, 124728.
23 R. V. Baier, J. I. Contreras Raggio, C. M. Giovanetti, H. Palza, I. Burda, G. Terrasi, B. Weisse, G. S. De Freitas, G. Nystrom, J. F. Vivanco and A. K. Aiyangar, *Biomater. Adv.*, 2022, **134**, 112540.
24 X. Chen, Q. Wu, J. Gao and Y. Tang, *Constr. Build. Mater.*, 2021, **296**, 123714.
25 S. Anitasari, C. Z. Wu and Y. K. Shen, *Bioengineering*, 2023, **10**, 305.
26 C. Jia, L. Wu, J. L. Fulton, X. Liang, J. J. De Yoreo and B. Guan, *J. Phys. Chem. C*, 2021, **125**, 3415–3420.
27 M. La Bella, R. Besselink, J. P. Wright, A. E. S. Van Driessche, A. Fernandez-Martinez and C. Giacobbe, *J. Appl. Crystallogr.*, 2023, **56**, 660–672.
28 X. Song, P. Zhang, B. Luo, K. Li, Y. Liu, S. Wang, Q. Wang, J. Huang, X. Qin, Y. Zhang, G. Zhou and D. Lei, *Adv. Sci.*, 2024, **11**, e2405420.
29 S. C. Endres, L. C. Ciacchi and L. Mädler, *J. Aerosol Sci.*, 2021, **153**, 105719.
30 A. E. Van Driessche, T. Stawski and M. Kellermeier, *Chem. Geol.*, 2019, **530**, 119274.
31 D. Aggarwal, V. Kumar and S. Sharma, *J. Biomed. Mater. Res., Part B*, 2023, **111**, 1232–1246.
32 X. F. Sanchez-Romate, J. Martin, A. Jimenez-Suarez, S. G. Prolongo and A. Urena, *Polymer*, 2020, **190**, 122236.
33 D. Li, X. Guo, H. Du, W. Ding, M. Li and Y. Xu, *J. Mech. Behav. Biomed. Mater.*, 2023, **147**, 106144.
34 Q. Lei, S. Gao, N. Sun, T. Zhang, L. Xiao, H. Huang, Y. Chen, L. Cai and F. Yan, *Mater. Des.*, 2024, **238**, 112732.
35 M. Bartnikowski, A. Abdal-Hay, N. J. Bartnikowski, Y. K. Kim and S. Ivanovski, *Appl. Surf. Sci.*, 2021, **555**, 149602.
36 S. Tajvar, A. Hadjizadeh and S. S. Samandari, *Int. Biodeterior. Biodegrad.*, 2023, **180**, 105599.
37 A. A. Menarbazari, A. Mansoori-Kermani, S. Mashayekhan and A. Soleimani, *Int. J. Biol. Macromol.*, 2024, **265**, 130827.
38 M. A. A. Ansari, P. K. Jain and H. S. Nanda, *J. Biomater. Sci., Polym. Ed.*, 2023, **34**, 1408–1429.
39 P. Tan, Y. Hua, B. Yuan, X. Liu, X. Chen, W.-N. Zeng, Q. Zeng, X. Zhu and X. Zhang, *J. Mater. Chem. B*, 2024, **12**, 7591–7603.
40 B. Ragini, S. Kandhasamy, J. P. Jacob and S. Vijayakumar, *Bioprocess Biosyst. Eng.*, 2024, **47**, 23–37.
41 Y. Zou, Y. Wang, J. Wang, S. Wang, L. Chen, Y. Xi, R. Xie, J. Yang and X. Xiao, *RSC Adv.*, 2024, **14**, 26103–26114.
42 L. Wang, C. Xu, K. Meng, Y. Xia, Y. Zhang, J. Lian, X. Wang and B. Zhao, *ACS Biomater. Sci. Eng.*, 2022, **9**, 165–181.